



# REPRODUCING THE CORRELATIONS OF TYPE C LOW-FREQUENCY QUASI-PERIODIC OSCILLATION PARAMETERS IN XTE J1550–564 WITH A SPIRAL STRUCTURE

PEGGY VARNIERE<sup>1</sup> AND FREDERIC H. VINCENT<sup>2</sup>

<sup>1</sup> APC, AstroParticule et Cosmologie, Université Paris Diderot, CNRS/IN2P3, CEA/Irfu, Observatoire de Paris, Sorbonne Paris Cité, 10, rue Alice Domon et Lonie Duquet, F-75205 Paris Cedex 13, France; [varniere@apc.univ-paris7.fr](mailto:varniere@apc.univ-paris7.fr)

<sup>2</sup> Observatoire de Paris/LESIA, 5, place Jules Janssen, F-92195 Meudon Cedex, France

Received 2016 July 20; revised 2016 November 16; accepted 2016 December 2; published 2017 January 13

## ABSTRACT

While it has been observed that the parameters intrinsic to the type C low-frequency quasi-periodic oscillations are related in a nonlinear manner among themselves, there has been, up to now, no model to explain or reproduce how the frequency, the FWHM, and the rms amplitude of the type C low-frequency quasi-periodic oscillations behave with respect to one another. Here we are using a simple toy model representing the emission from a standard disk and a spiral such as that caused by the accretion–ejection instability to reproduce the overall observed behavior and shed some light on its origin. This allows us to prove the ability of such a spiral structure to be at the origin of flux modulation over more than an order of magnitude in frequency.

*Key words:* accretion, accretion disks – black hole physics – stars: individual (XTE J1550–564) – stars: oscillations

## 1. INTRODUCTION

Black hole binaries exhibit highly variable light curves, especially in X-rays. Since their first detection, there has been a long string of efforts to understand the source of this variability. Up to now, no model has gained wide acceptance, especially concerning the strong and highly variable low-frequency quasi-periodic oscillation (LFQPO), which appears as a narrow peak in the 0.1–30 Hz range of the power density spectrum (PDS) of outbursting sources and can attain a strong rms amplitude. Among the distinct models proposed to describe them, many imply a structure orbiting the disk causing the X-ray modulation. Such structures include precessing tori (Schnittman et al. 2006; Ingram et al. 2009), hot spots (Karas et al. 1992; Schnittman & Bertschinger 2004; Tagger & Varniere 2006; Pechacek et al. 2013), or spirals (Tagger & Pellat 1999; Varniere et al. 2002). Here we will focus on the latter case with a toy model based on the accretion–ejection instability (AEI).

In the many steps done in order to further our understanding of the mechanism at the origin of the QPOs, the most common is the search for correlations, which models would in turn need to explain. Indeed, temporal features of the PDS, such as QPO frequencies, are correlated with spectral features (Muno et al. 1999; Remillard et al. 2002; Rodriguez et al. 2002, 2004; Vignarca et al. 2003), or other temporal features such as breaks or other QPOs, but the way the intrinsic parameters of such a feature relate to one another is rarely explored. Recently, Motta et al. (2015) explored the behavior of LFQPOs in several sources and in particular showed that the rms versus frequency tends to show both positive and negative correlations when looking at type C LFQPOs.<sup>3</sup> While the declining, negative side of the correlation seems quite similar for outbursts of the same source, the positive side of the correlation varies more and the slope can get close to zero. Up to now no model has tried giving an explanation as to why this curve is thus shaped and what it means. Here we are using a simple toy model representing one of the instabilities proposed to explain the

LFQPO, the AEI, to reproduce the observed behavior and shed some light on its origin.

We will first look in more detail at how the LFQPO parameters relate to one another for XTE J1550–564 in the case of the well-documented outburst of 1998–99 and the one of 2000 for comparison. Taking advantage of the long outburst and the numerous observations in 1998–99, we aim to have a good description of the LFQPO parameters’ behavior over close to 2 decades in frequency. Then we will present our simple model mimicking the AEI, and in the last section we will compare this model with observed data from XTE J1550–564 and show how the model’s parameters can be adjusted to give a good representation of the observed data.

## 2. THE 1998–99 OUTBURST OF XTE J1550–564

In order to run simulations reproducing the behavior pointed out by Motta et al. (2015), we first had to obtain an observational curve for one outburst of one source. Indeed, by using one source we are freeing ourselves from the impact of the mass of the object, which determines how a frequency relates to a position in the disk, and by using one outburst we are freeing ourselves from possible differences in the system itself, as the exact values of magnetic field, density, and other physical parameters can change widely from one outburst to the next (and possibly be the reason behind a “failed outburst”).

We choose to focus on the 1998–99 outburst of XTE J1550–564, which was simultaneously long, extremely bright, and well documented in the literature, hence freeing us from the need to reduce data, as all are available in publications such as Sobczak et al. (2000) and Remillard et al. (2002), from which all the observational data presented here are from. Here we are only interested in the timing analysis, and, as in Motta et al. (2015), we are restraining ourselves to type C LFQPOs. From the fit of the main QPO peak in the PDS one gets its frequency,  $\nu_{\text{QPO}}$ , its rms amplitude, and its FWHM.

If one looks at the time evolution of those three quantities during the outburst (see Figure 1), we see that the QPO starts with a very low frequency, a small width (understandable as the frequency is small), and a relatively high rms amplitude. Then the QPO frequency and width increase, in a seemingly similar

<sup>3</sup> The data for type B are more limited and over a smaller range of frequencies that do not allow us to make a conclusion on the possible shape.

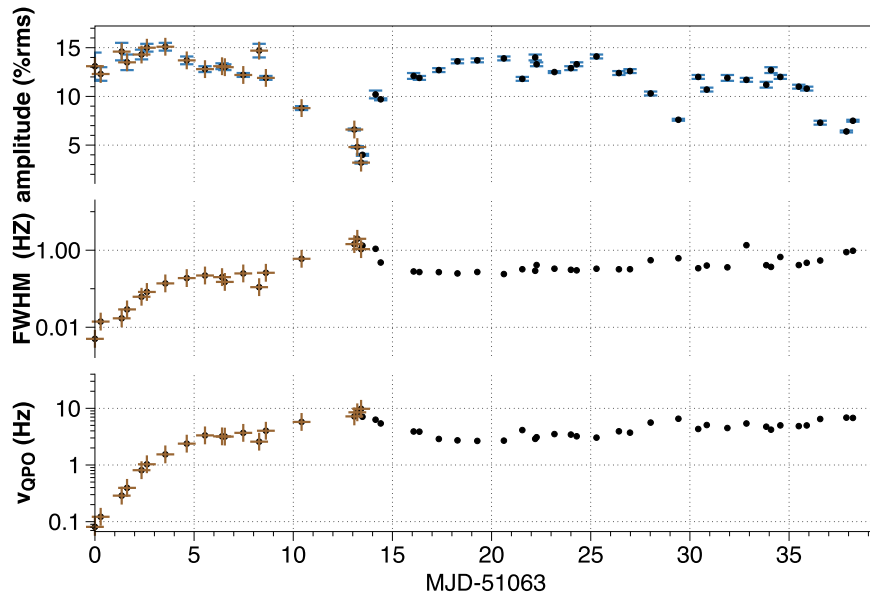


**Figure 1.** Evolution of the rms amplitude, FWHM, and frequency of the type C LFQPO during XTE J1550–564 as a function of the day since the start of the 1998–99 outburst. The brown plus signs represent the evolution of the QPO until it reaches its maximum frequency for the first time.

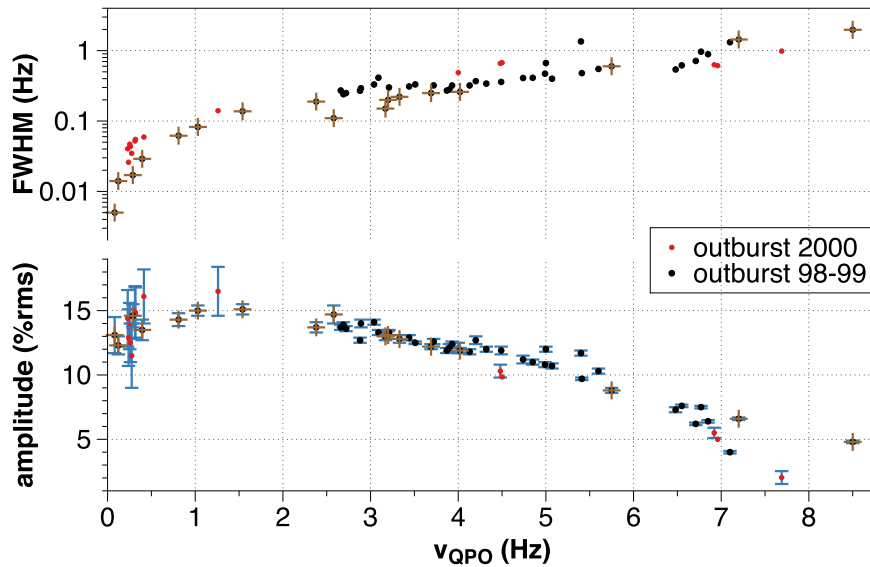


**Figure 2.** Evolution of the rms amplitude and FWHM as a function of the type C LFQPO frequency during the XTE J1550–564 outburst of 1998–99. As in the previous figure, the brown plus signs represent the first pass of the QPO on the curve before returning to lower frequencies. For comparison the red points represent the evolution during the 2000 outburst.

way, while its rms stays relatively high until the LFQPO frequency hits a few hertz. Then the rms starts decreasing, reaching a minimum when the QPO frequency and width reach a maximum. After reaching its maximum (shown by the brown plus signs), the QPO frequency exhibits slow variations between 7 and 2.5 Hz. It is interesting to note that while the QPO frequency is relatively stable, so are both the width and rms of the QPO, hinting at a linked behavior.

To explore that, and following the work of Motta et al. (2015), we decided to see how those parameters of the QPO in the PDS correlate with one another. The lower plot of Figure 2 shows how the rms behaves as a function of the QPO frequency. We see that for our chosen object and outburst the shape of the curve is not as pronounced as the one in Motta et al. (2015). This is due to the fact that in Motta et al. (2015)

there are 17 outbursts for six different objects, represented and averaged on the same plot. To better compare, we added as red dots the value from the 2000 outburst of XTE J1550–564, which has a steeper increase of rms for the lowest frequency values, though with large error bars, while having a similar behavior for higher frequencies. This diversity of behavior explains the difference between our plot and the one from Motta et al. (2015), which contains data from not only several outbursts but also objects. By being able to reproduce the behavior with a model based on the AEI, we aim to explain those differences and similitudes and on what do they depend.

In the case of the 1998–99 outburst the evolution with the QPO frequency is well sampled and the shape of the curve is similar to that seen in Motta et al. (2015), starting with a positive, albeit small, slope, a maximum reached for an LFQPO

frequency of about 1.5 Hz with an associated rms of about 15%, and then a negative correlation up to a frequency of 10 Hz. We see that the brown plus signs representing how the QPO first reaches its maximum also represent the first pass on the rms versus frequency curve. The upper plot of Figure 2 shows how the FWHM of the peak behaves as a function of its frequency. While it always keeps a positive correlation, meaning that the width of the peak is increasing with its frequency, the actual slope is varying. The behavior during the 2000 outburst is similar, but the peak in the PDS is almost always larger than during the 1998–99 outburst.

The challenge for a model is to be able to give meaning to both of those plots simultaneously, especially focusing on the the origin of the change of sign in the correlation.

### 3. AN EVOLVING SPIRAL TO MIMIC THE AEI

Here we are concentrating on one model that has been proposed to explain the LFQPO based on the AEI (Tagger & Pellat 1999). The AEI is a global instability occurring in the inner region of a magnetized disk close to the equipartition, namely, when the magnetic pressure is of the order of the gas pressure. It is characterized by a spiral wave developing in the inner region of the disk. At the corotation radius between the accreting gas and the spiral wave, a Rossby vortex develops and stores accretion energy and angular momentum. In the presence of a low-density corona the Rossby vortex will twist the footpoint of the magnetic field lines. This causes an Alfvén wave to be emitted toward the corona, therefore linking accretion and ejection (Varniere & Tagger 2002).

#### 3.1. AEI and Outburst

The first attempt to use the AEI to improve our understanding of QPO evolution, and hence follow the evolution of the source, was the “Magnetic Flood Scenario” (MFS) done for the  $\beta$  class of GRS 1915+105 (Tagger et al. 2004) and then expanded to encompass the evolution along the hardness–intensity diagram (HID; Varniere et al. 2007). This was the first step in expanding the model toward classifying black hole states (Varniere et al. 2011) and a possible explanation for the different types of LFQPOs (Varniere et al. 2012).

This extended MFS focuses on explaining the behavior along the HID diagram using a limit cycle determined by the advection and destruction, via magnetic reconnection, of poloidal magnetic flux in the inner region of the disk. As the condition in the disk changes, different sets of instabilities become dominant (Varniere et al. 2011), causing the different behavior and state transition observed. In that scenario the magnetorotational instability (Balbus & Hawley 1991) dominates in the soft states, while during the low state, the AEI is at the origin of the LFQPO and sends energy toward the corona by means of Alfvén waves.

If we assume the starting configuration where the magnetic flux stored around the black hole and the disk flux are parallel, the disk inner radius is large and accretion remains weak. To start the outburst, something needs to change. Now let us assume a field reversal (dynamo in the disk or the companion) in the flux advected in the disk; we obtain a slow decrease of the stored flux, and at the same time the inner radius of the disk decreases. During all that time, the AEI is present in the disk, and the source is in the low-hard state. At that point there are two possibilities: no field reversal occurs until all the stored

flux is canceled by the disk flux, we obtain a global reconfiguration of the magnetic field, which favors an ejection and the disk is back at its last stable orbit, or there is a field reversal before that and we obtain a failed flare as seen sometimes. Slowly the stored flux is rebuilt, parallel to the disk one, up to a strong stored flux that is the same as the initial configuration but in the opposite direction, hence being ready for another outburst.

#### 3.2. Parameterization of the Disk Temperature Profile

As in Varniere & Vincent (2016), we will not enter into the details of the instability, but we will use a simple model to mimic the spiral emerging from the AEI as seen in numerical simulations (see, e.g., Varniere et al. 2012). We consider a geometrically thin disk surrounding a Schwarzschild black hole of mass  $M$  taken to be  $10.5 M_{\odot}$  for XTE J1550–564. The disk extends from a varying inner radius  $r_{\text{in}}$  to a fixed outer radius  $r_{\text{out}} = 500 M$  so that it is larger than our observing window in every synthetic observation we perform. To keep a simple structure, we choose to have the temperature profile  $T_0(r) \propto r^{-\eta}$ . In agreement with the thin-disk blackbody model, we took  $\eta = 0.75$  as the equilibrium temperature profile. The equilibrium temperature profile is fixed by choosing the temperature at the last stable circular orbit (LSO), labeled  $T_{\text{LSO}}$ .

On top of this equilibrium disk we model the consequences of the presence of the AEI in a very simple way, just describing the hotter spiral structure rotating in the equilibrium disk, in agreement with numerical simulations of the AEI. The temperature of the disk with this added spiral feature reads

$$T(t, r, \varphi) = T_0(r) \times \left[ 1 + \gamma \left( \frac{r_c}{r} \right)^{\beta} \exp \left( -\frac{1}{2} \left( \frac{r - r_s(t, \varphi)}{\delta r_c} \right)^2 \right) \right]^2, \quad (1)$$

where the perturbation term between brackets describes the spiral pattern on top of the standard power-law profile. The parameter  $\gamma$  encodes the temperature contrast between the spiral and the surrounding disk. The quantity  $r_c$  is the corotation radius of the spiral. The spiral temperature is thus following a power-law decrease when moving away from  $r = r_c$ , with an exponent  $\beta$ . This ensures that the spiral will fade away into the disk after a few turns. In the last, Gaussian term,  $r_s$  is a shape function encoding the spiral feature. It ensures that the spiral’s width is a factor  $\delta$  times the corotation radius. The shape function reads

$$r_s(t, \varphi) = r_c \exp(\alpha(\varphi - \Omega(r_c)t)), \quad (2)$$

where  $\alpha$  is the spiral opening angle and  $\Omega(r_c) = \sqrt{GM} r_c^{-1.5}$  is the Keplerian<sup>4</sup> frequency at  $r_c$ . Ultimately it is the rotation frequency of the spiral and the frequency at which the flux is modulated.

#### 3.3. Emission from the Disk and Ray Tracing

The whole disk is assumed to simply emit as a blackbody at the temperature  $T(t, r, \varphi)$ , namely, following  $B(\nu, T) = \frac{2h^2\nu^3}{c^2} / (e^{\frac{h\nu}{k_b T}} - 1)$ , with  $k_b$  the Boltzmann constant,  $\nu$  the

<sup>4</sup> In all the cases presented here  $r_c$  is always far enough from the last stable orbit for the rotation curve to be well approximated by the Keplerian case.

frequency,  $c$  the speed of light, and  $h$  the Planck constant. So the specific intensity emitted at some position in the disk is

$$I_{\nu}^{\text{em}} = B_{\nu}(\nu^{\text{em}}, T), \quad (3)$$

where the superscript em refers to the emitter’s frame, i.e., a frame corotating (at the local Keplerian frequency) with the disk. This emitted intensity is then transformed to the distant observer’s frame using the constancy along geodesics of  $I_{\nu}/\nu^3$ . Thus,

$$I_{\nu}^{\text{obs}} = g^3 I_{\nu}^{\text{em}}, \quad (4)$$

where  $g = \nu^{\text{obs}}/\nu^{\text{em}}$  is the redshift factor. This redshift factor is in particular responsible for the so-called beaming effect, which makes the observed specific intensity stronger when the emitter travels toward the observer and fainter in the opposite case.

To compute maps of specific intensity  $I_{\nu}^{\text{obs}}$ , we use the open-source general relativistic ray-tracing code GYOTO<sup>5</sup> (Vincent et al. 2011), into which we added the parameterized disk profile defined in the previous section. Null geodesics are integrated in the Schwarzschild metric, backward in time from a distant observer at some inclination with respect to the disk. Inclination is equal to the angle between the observer’s line of sight and the normal to the black hole’s equatorial plane. From such maps of specific intensity, the light curve (flux as a function of time) is derived by summing all pixels weighted by the element of solid angle subtended by each pixel.

Using this code, we will be able to compute the rms amplitude of any spiral structure as defined by our model in Equation (1). In order to compare with observations, we will first select a few QPO frequencies at which to compute the rms amplitude of the flux modulation coming from the presence of a spiral in the disk.

### 3.4. Choice of the Parameters

Some of the parameters only depend on the disk and can be set in agreement with observation, such as the fact that we want a geometrically thin disk whose aspect ratio we set at  $H/r = 0.01$ . It is also the case for the temperature at the LSO, which is taken to be  $T_{\text{LSO}} = 10^7$  K, thus emitting blackbody radiation mainly around 1 keV. While the exact flux computing depends on the chosen scaling for the temperature and the scaling of the disk, here we are interested in the amplitude of the modulation coming from the spiral that occurs “on top” of the equilibrium disk. We choose this temperature scaling in agreement with the temperature deduced from the spectral fit during the 1998–99 outburst of XTE J1550–564, when the inner edge of the disk is also found to be small (see, e.g., Remillard et al. 2002; Varniere et al. 2016).

The remaining parameters are specific to the spiral, some of which evolve with time, such as the amplitude of the spiral, its radial size, and its frequency, and some of which depend more on the disk parameters, such as the opening angle of the spiral and how fast it becomes drowned in the disk. In order to choose them, we are guided by previous numerical simulations (such as the one from Varniere et al. 2011, 2012) and freeze the one that depends on the disk to typical values. In that respect the opening angle is chosen to be  $\alpha = 0.1$ , while the power-law

exponent encoding the temperature decreases away from  $r = r_c$  and is set to  $\beta = 0.75$ . This ensures that the spiral will be negligible after a few turns and not run for the entire disk. The impact of those parameters on the total flux is actually linked, as for smaller opening angle more of the spiral is inside the emitting region (Varniere & Blackman 2005). Again we are interested in the rms amplitude of the modulation and not the total flux, and so we decided to fix those. Keeping them the same value for the entire set of simulations is equivalent to saying that the condition in the disk pertaining to the wave propagation stays similar.

As shown by Tagger & Pellat (1999), the corotation radius of the spiral is a few times the inner radius of the disk. Here we chose to keep  $r_c/r_{\text{in}}$  fixed at a typical value of 2; thus, as the inner radius varies, so does the corotation radius, which determines the frequency of the QPO, which is a trend in agreement with observations (Varniere et al. 2002; Mikles et al. 2006). This is actually a strong constraint that we are imposing, as the actual value where the corotation is with respect to the inner edge of the disk does not stay constant during a full outburst, but changes with the physical parameters of the disk, such as its density and magnetic field strength. We take a simplified approach, assuming that the disk conditions do not change dramatically, as we are trying to reduce as much as possible the number of parameters in order to fit the observational curves of the QPO behavior. Changing this value has no consequences on the emission coming from the spiral; it represents the unmodulated flux from the disk between the inner edge of the disk and the corotation radius. Hence, it is changing the total flux on top of which is the modulation. In order to constrain this directly from observation, we will need to wait for instruments like NICER (Gendreau et al. 2012).

From those choices we see that there are still three parameters that are needed in order to compute the emission and ultimately by how much the flux is modulated.

1. The position of the corotation,  $r_c$ , which is a direct link to the frequency at which the QPO will be. Indeed, the spiral wave will rotate at  $\Omega(r_c)$ , hence modulating the flux at that frequency. This is the first hypothesis of our association between the AEI and the mechanism at the origin of the QPO. For this paper we will have  $r_c$  varying between 8.75 and 60  $r_{\text{LSO}}$ , which converts into more than one order of magnitude in frequency between 0.47 and 8.5 Hz. While smaller frequencies are observed in early parts of the outburst, they would require a much larger disk and a tremendous increase in computation time. We therefore choose to start our sample of simulated light curves at a frequency of  $\nu = 0.47$  Hz, which already allows us to see both sides of the correlation.
2. The width of the structure,  $\delta$ , which represents the radial thickness of the spiral arm at the corotation radius. It is the uncertainty in its position and can be translated, similarly to  $r_c$ , into an extension in frequency space, namely, the FWHM of the observed peak.
3. The height of the structure,  $\gamma$ , which is related to the amplitude of the instability in the disk and will, along with  $\delta$ , govern the final modulation of the flux from the spiral. This last parameter has its own set of constraints that need to be fulfilled, as it represents the growth of the instability with time.

<sup>5</sup> GYOTO can be downloaded at <http://gyoto.obspm.fr>.

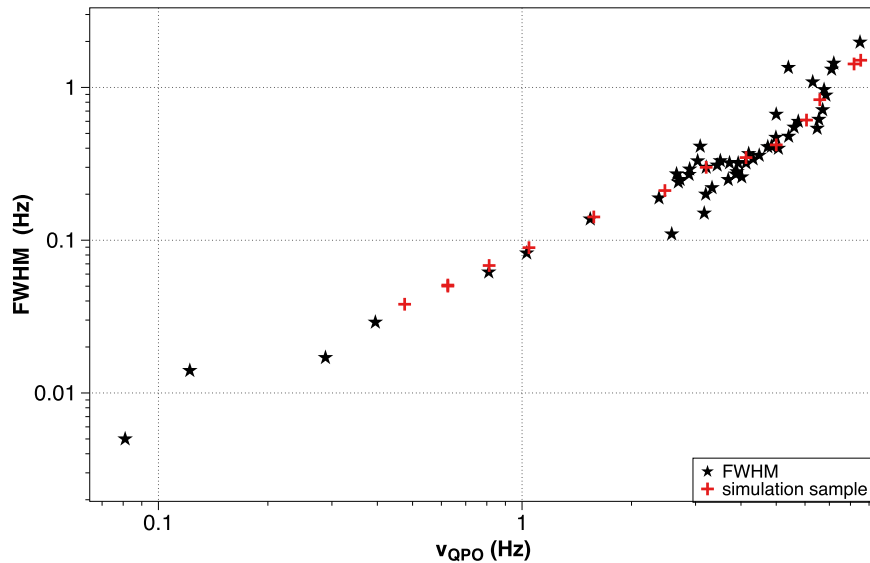


**Figure 3.** Correlation between the frequency of the QPO and FWHM of the LFQPO in the case of the XTE J1550–564 outburst of 1998–99 (black stars) and in the case of our simulated sample (red plus signs).

#### 4. REPRODUCING THE BEHAVIOR OF QPO PARAMETERS

Our aim here is to check whether a spiral structure similar to the one from the AEI is able to reproduce the observed behavior of the LFQPOs as seen in Figure 2. In that respect we need to define a set of frequencies that provide a good representation of the observation at which we will then compute the emission and modulation of the flux that one would observe from the AEI. As explained in the previous section, we have three parameters to vary in order to adjust the behavior of LFQPOs’ observables. Some of those, like the pair position/frequency of the structure  $\Omega(r_c)$ , do not allow any degree of freedom when we want to compute the behavior at a particular frequency. The only requirement is that the corotation value associated is indeed inside the disk. Others, such as  $\gamma$ , have a set of constraints that come from the nature of the instability we are studying. Indeed, as the AEI grows in the disk, so does the spiral, and that until the instability reaches saturation. The growth rate of the instability is related to the physical conditions in the disk and stays the same until saturation. As  $\gamma$  is a measure of this growth, it needs to reflect this behavior with an initial linear growth and then a saturation.

##### 4.1. FWHM versus Frequency: Selecting Our Sample

In order to select the sample of frequencies at which we will compute the rms amplitude, we first decide on the range in which we aim to provide a good description of the data. We choose to focus on [0.47, 8.5] Hz as it is wide enough to follow the behavior on both sides of the break and is also computationally reasonable.

In Equation (1) we see that  $\delta$  is the parameter controlling how wide is the spiral around the corotation radius. In a similar fashion to how  $r_c$  is related to the frequency of the modulation  $\Omega(r_c)$ , the observable to which  $\delta$  is closely related is the FWHM<sup>6</sup> of the QPO. Indeed, as the QPO frequency is related to the rotation frequency at  $r_c$ , the actual radial thickness of the

spiral arm will cause a small uncertainty in the associated frequency,  $3\Omega(r_c)\sqrt{2\ln 2}/(2\delta r_c)$ .

We therefore choose our sample as shown in Figure 3, where the points corresponding to the parameters of our simulation are represented as red plus signs among the black stars of XTE J1550–564 observations. It is interesting to note that on a log-log diagram there is a mostly linear relation, though with some dispersion above 2 Hz, between the FWHM and the frequency.

We now need to check that our selected sample of frequencies and associated FWHM are indeed a good representation of the observed distribution. As both sets, our sample and the observations, do not have matching abscissa, we cannot do a direct comparison. We first need to fit one set of data and then check how that fit is performing as a fit for the other set. The first few points of the outburst, at very small frequencies/high  $r_c$ , which are outside the boundary of our sample, are mostly coherent with the behavior extrapolated from our limited sample, and as a result, our sample set gives an acceptable representation of the observational set, following its shape for more than one order of magnitude and with a  $\chi^2 = 0.93$  for the fit of all the observational data of our sample.

##### 4.2. Evolution of the Spiral Strength as the Outburst Evolves

Now that we have selected a set of QPO values representative of the observed sample, we need to compute their rms amplitude. For that we need to focus on the parameter  $\gamma$ , which reflects the amplitude of the spiral in the disk. As it represents the growth of the instability, we have constraints on its evolution as a function of time. It will increase linearly at a rate that depends on the local disk condition until reaching saturation. In order to calibrate this behavior, we use two data points from the early part of the outburst. Here we are making the assumption that the local conditions in the disk do not change widely during the “type C LFQPO stage” of the outburst. In order to ensure this as much as possible, we are focusing on the subset of observational points that represent the first “pass” on the curve, represented by the brown plus signs in

<sup>6</sup> For a Gaussian  $e^{-x^2/(2\sigma^2)}$  the FWHM is  $2\sqrt{2\ln 2}\sigma$ .

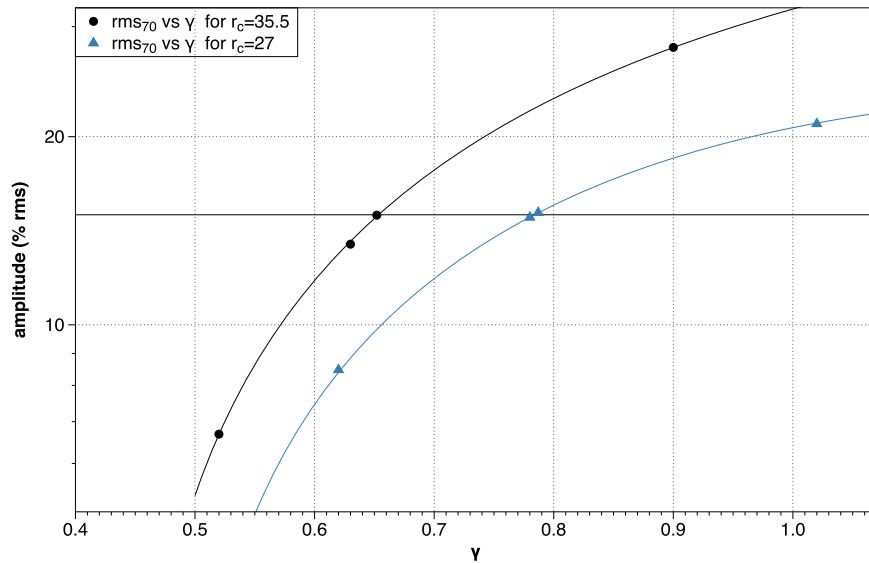


**Figure 4.** Evolution of the rms as a function of  $\gamma$  for two different positions of the spiral, meaning two different QPO frequencies. The horizontal line at 15 Hz represents the aim of rms amplitude for the 1.03 Hz modulation.

Figures 1 and 2, to adjust to our simulated data.<sup>7</sup> This represents about the first 12 days of the outburst. Once we have the behavior for the first pass, we will, as was done for the FWHM in Figure 3, use the full sample to check whether those points are a good representation of the 1998–99 outburst of XTE J1550.

In order to calibrate the curve of the  $\gamma$  evolution, we choose points in the early part of the outburst:

- (1) with  $\nu_{\text{QPO}} = 1.03$  Hz with an rms of 15% and  $Q = 6.98$ ; and
- (2) with  $\nu_{\text{QPO}} = 1.54$  Hz with an rms of 15.1% and  $Q = 11.2$ .

For those two cases, we then determine the spatial parameters for each of the spiral, namely: (1)  $r_c = 35.5 r_{\text{LSO}}$ , which gives a frequency of  $\sim 1.04$  Hz and a  $\delta$  of 0.295, and (2)  $r_c = 27 r_{\text{LSO}}$ , which gives a frequency of  $\sim 1.57$  Hz and a  $\delta$  of 0.28. We then run one set of simulations to compute the emission in each case, exploring the rms of the detected modulation as a function of  $\gamma$ . As shown in Figure 4, this allowed us to pinpoint the  $\gamma$  necessary for the observational data: (1)  $\gamma = 0.652$  and (2)  $\gamma = 0.787$ . In order to get the evolution of  $\gamma$  as a function of time, we perform a fit of the observed behavior of the frequency of the QPO as a function of time for the first 12 days of the outburst, which correspond to the first pass on the rms =  $f(\nu_{\text{QPO}})$ . This allows us to associate a time with each member of our simulated set, depending on the frequency they are matching in the observation. This in turn gives us a good estimate of the slope of the evolution of  $\gamma$ , which has to be linear for this instability.<sup>8</sup> We then can “let the instability grow” along this line, meaning that we slowly increase the parameter  $\gamma$  as the corotation radius decreases to match the change in frequency. This is valid until we reach the saturation point when  $\gamma$  becomes a constant. The evolution of  $\gamma$

<sup>7</sup> Indeed, during the outburst the evolution on the rms =  $f(\nu_{\text{QPO}})$  curve is always the same, starting on the far left and moving up to the far right, followed by a series of oscillations up and down the right branches. The end of the first “pass” seems to be concurrent with the maximum of the outburst/state change.

<sup>8</sup> It is only an estimate, as it is hard to pinpoint the exact observed value with our simulations.

coming from our sampled light curves is given in the inset of Figure 5.

This growth of  $\gamma$  will in turn increase the amplitude of the modulation created by the growing spiral, in agreement with the observed behavior in XTE J1550–564 seen in Figure 2. While we continue to increase the amplitude of the spiral as the inner edge of the disk slowly approaches the black hole to match the observed frequency, we see in Figure 5 that the overall amplitude of the modulation actually decreases for LFQPOs of frequency higher than 2 Hz even if the  $\gamma$  continue to increase until the frequency of the modulation reaches about 3.5 Hz.

Before looking in more detail at the cause of this change, we need to compare the resulting rms distribution of our sample set with the observed data to test whether we have good agreement. As we have two sets of data points that do not have similar abscissas, we first need to perform a fit of the simulated data points. We performed a simple polynomial fit of our sample set, which results in the red line shown in Figure 5. This is a fit of the 12 simulated rms amplitudes represented by the red plus signs. Once we had this curve, we tested whether it was also a good representation of the observed data. This is not a fit in the sense that the red curve is not modified to adjust the observational point; we directly use the curve coming from the simulated rms, but we can still use the same tool to assess the quality of the representation. The bottom of Figure 5 shows the residual obtained when using the fit of the red plus signs to adjust all the observational data within the domain of validity of the fit, meaning all the observed type C LFQPOs above 0.4 Hz of the 1998–99 outburst of XTE J1550–564. The associated  $\chi^2$  obtained is 0.94.

In order to compute the adequation of the curve to the observational data, we used the entire data set of observations and not just the initial subset representing the first 12 days of the outburst (namely, the first pass on the curve). When fitting only the first pass on the observational curve to our simulated data, we improve the agreement with  $\chi^2 = 0.98$ , which means that the conditions in the disk are indeed changing as the system is oscillating along the right branch of the rms =  $f(\nu_{\text{QPO}})$ , but the initial conditions are still a good

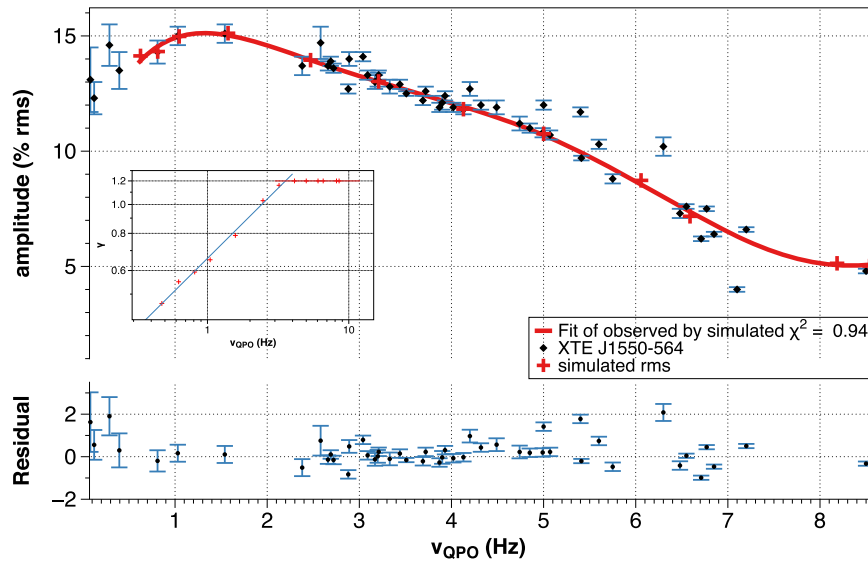


**Figure 5.** Correlation between the rms and frequency of the LFQPO in the case of the XTE J1550–564 outburst of 1998–99 (black star) and in the case of our simulated light curves (red plus signs). The red line is a polynomial fit of the simulated data, and the bottom shows the residual between this simulated profile and the observed data, which gives a  $\chi^2 = 0.94$ . The inset on the left represents the associated evolution of  $\gamma$  as a function of  $\nu_{\text{QPO}}$ .

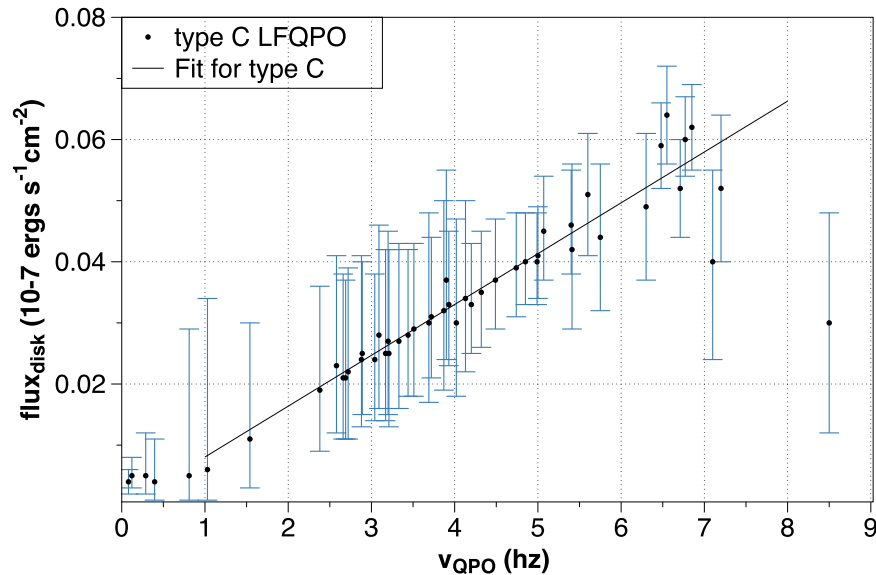


**Figure 6.** Flux of the disk as a function of the LFQPO frequency during the 1998–99 outburst.

approximation. The change in the disk condition would then explain the dispersion one gets for observables taken later in the outburst. Similarly, comparing the behavior between the 1998–99 outburst and the one of 2000 would tend to hint that the change in the system is causing the difference in the  $\text{rms} = f(\nu)$  curve. It would be interesting to look at the differences in the case of failed outbursts as well, though there is not enough data at the moment to construct such a curve.

#### 4.3. Increase of the Spiral Strength but Decrease in rms

As we have a good representation of the  $\text{rms} = f(\nu_{\text{QPO}})$  with our toy model, we can look at the reason why the rms of the modulation is decreasing while the strength of the spiral is still increasing. In our model, this is due to the fact that, as the inner edge of the disk gets closer to the black hole, the “unmodulated” part of the disk, namely, between  $r_{\text{in}}$  and  $r_c = 2r_{\text{in}}$ , gets hotter, so its overall contribution to the total flux

increases. This can be easily checked in observation. During the outburst of XTE J1550–564, we see in Figure 6 that an increase of the disk flux was detected concurrently to the increase in the QPO frequency.

This causes a decrease in the rms of the QPO even while the spiral amplitude is steadily increasing. From those simulations we see that the actual rms of an LFQPO is not solely related to the strength of the mechanism at its origin but comes from a competition between

1. the actual strength of the instability responsible for the LFQPO and
2. the unmodulated flux emitted between the inner edge of the disk and the corotation radius of the instability.

While this implies that all outbursts will have a similar increase and then decrease, the actual shape of the curve and the position of the maximum rms will depend on the physical

state of the disk and so can vary between outbursts of the same source and a fortiori between sources. Indeed, the growth rate of the instability depends on the physical state of the disk (such as its density, magnetization, etc.), which has no reason to stay the same between outbursts. It would be interesting to see how failed outbursts behave when plotted on those  $\text{rms} = f(\nu_{\text{QPO}})$  curves. It might give us an insight on the differences inside the disk that cause the outburst to fail.

## 5. CONCLUSIONS

In this paper we explored how a toy model based on the AEI, namely, the presence of a spiral, could give a good representation of the LQPO behavior during a full outburst. We were able to adjust the observed  $\text{rms} = f(\nu_{\text{QPO}})$  curve for the 1998–99 outbursts of XTE J1550–564 with a  $\chi^2 = 0.94$ , confirming the AEI as a good candidate to explain the LFQPO.

From those simulations we see that the actual rms of an LFQPO comes from two competing mechanisms.

1. First of all, along with the disk getting closer to the last stable orbit during the outburst, the instability responsible for the LFQPO is also getting stronger; hence, we have a higher rms as the frequency increases.
2. But as the disk gets closer to its last stable orbit, the unmodulated flux emitted between the inner edge of the disk and the corotation radius increases, while the instability slowly reaches saturation, hence creating a slow decrease in the rms amplitude as the frequency further increases.

This means that for a different outburst of the same source one can expect a similar curve but with a different position for its maximum. Indeed, this will depend on the strength of the instability, which in turn depends on the local condition in the disk. This could help shed some light on failed outbursts by looking at how the LFQPO's parameters behave from the start and what it says about the condition in the disk.

P.V. acknowledges financial support from the UnivEarthS Labex program at Sorbonne Paris Cité (ANR-10-LABX-0023 and ANR-11-IDEX-0005-02). Computing was done using the FAcE (Francois Arago Centre) in Paris.

## REFERENCES

- Balbus, S. A., & Hawley, J. F. 1991, *ApJ*, **376**, 223
- Gendreau, K. C., Arzoumanian, Z., & Okajima, T. 2012, *Proc. SPIE*, **8443**, 84434V
- Ingram, A., Done, C., & Fragile, P. C. 2009, *MNRAS*, **397**, L101
- Karas, V., Vokrouhlicky, D., & Polnarev, A. G. 1992, *MNRAS*, **259**, 569
- Mikles, V. J., Eikenberry, S. S., & Rothstein, D. M. 2006, *ApJ*, **637**, 978
- Motta, S. E., Casella, P., Henze, M., et al. 2015, *MNRAS*, **447**, 2059
- Muno, M. P., Morgan, E. H., & Remillard, R. A. 1999, *ApJ*, **527**, 321
- Pechacek, T., Goosmann, R. W., Karas, V., Czerny, B., & Dovciak, M., 2013, *A&A*, **556**, A77
- Remillard, R. A., Sobczak, G. J., Muno, M. P., & McClintock, J. E. 2002, *ApJ*, **564**, 962
- Rodriguez, J., Corbel, S., Hannikainen, D. C., et al. 2004, *ApJ*, **615**, 416
- Rodriguez, J., Varniere, P., Tagger, M., & Durouchoux, P. 2002, *A&A*, **387**, 487
- Schnittman, J. D., & Bertschinger, E. 2004, *ApJ*, **606**, 1098
- Schnittman, J. D., Homan, J., & Miller, J. M. 2006, *ApJ*, **642**, 420
- Sobczak, G. J., McClintock, J. E., Remillard, R. A., et al. 2000, *ApJ*, **531**, 537
- Tagger, M., & Pellat, R. 1999, *A&A*, **349**, 1003
- Tagger, M., & Varniere, P. 2006, *ApJ*, **652**, 1457
- Tagger, M., Varniere, P., Rodriguez, J., & Pellat, R. 2004, *ApJ*, **607**, 410
- Varniere, P., & Blackman, E. G. 2005, *NewA*, **11**, 43
- Varniere, P., Mignon-Risse, R., & Rodriguez, J. 2016, *A&A*, **586**, 6
- Varniere, P., Rodriguez, J., & Tagger, M. 2002, *A&A*, **387**, 497
- Varniere, P., & Tagger, M. 2002, *A&A*, **394**, 329
- Varniere, P., Tagger, M., & Rodriguez, J. 2011, *A&A*, **525**, A87
- Varniere, P., Tagger, M., & Rodriguez, J. 2012, *A&A*, **545**, 40
- Varniere, P., Tagger, M., Rodriguez, J., & Cadolle Bel, M. 2007, in Proc. Annual Meeting of the French Society of Astronomy and Astrophysics, ed. J. Bouvier, A. Chalabaev, & C. Charbonnel, 221
- Varniere, P., & Vincent, F. H. 2016, *A&A*, **591**, 36
- Vignarca, F., Migliari, S., Belloni, T., Psaltis, D., & van der Klis, M. 2003, *A&A*, **397**, 729
- Vincent, F. H., Paumard, T., Gourgoulhon, E., & Perrin, G. 2011, *CQGra*, **28**, 225011